FINITE ELEMENT SIMULATION OF SINGLE-LAP SHEAR TESTS UTILIZING THE COHESIVE ZONE APPROACH

by

WILSON PEREZ

A thesis submitted in partial fulfillment of the requirements
for the Honors in the Major Program in Mechanical Engineering
in the College of Engineering and Computer Science
and in the Burnett Honors College
at the University of Central Florida
Orlando, Florida

Spring Term, 2016

Thesis Chair: Dr. Ali P. Gordon, Ph.D.

Abstract

Many applications require adhesives with high strength to withstand the exhaustive loads encountered in regular operation. In aerospace applications, advanced adhesives are needed to bond metals, ceramics, and composites under shear loading. The lap shear test is the experiment of choice for evaluating shear strength capabilities of adhesives. Specifically during single-lap shear testing, two overlapping rectangular tabs bonded by a thin adhesive layer are subject to tension. Shear is imposed as a result. Debonding occurs when the shear strength of the adhesive is surpassed by the load applied by the testing mechanism. This research develops a finite element model (FEM) and material model which allows mechanicians to accurately simulate bonded joints under mechanical loads. Data acquired from physical tests was utilized to correlate the finite element simulations. Lap shear testing has been conducted on various adhesives, specifically SA1-30-MOD, SA10-100, and SA10-05, single base methacrylate adhesives. The adhesives were tested on aluminum, stainless steel, and cold rolled steel adherends. The finite element model simulates what is observed during a physical single-lap shear test consisting of every combination of the mentioned materials. To accomplish this, a three-dimensional model was created and the cohesive zone approach was used to simulate debonding of the tabs from the adhesive. The thicknesses of the metallic tabs and the adhesive layer were recorded and incorporated into the model in order to achieve an accurate solution. From the data, force output and displacement of the tabs are utilized to create curves which were compared to the actual data. Stress and strain were then computed and plotted to verify the validity of the simulations. The modeling and constant determination approach developed here will continue to be used for newly-developed adhesives.

Dedication

For my family and friends who stay by my side in the good times and bad. This work is dedicated to those who made this possible and supported me every step of the way.

Acknowledgments

I would like to thank my thesis chair, Dr. Ali P. Gordon for pushing me to complete this thesis. Dr. Gordon saw something in me that I could not even see myself. Due to his support, I was able to meet the requirements for completing the Honors in the Major program and this work has inspired me to pursue a Ph.D. in the field of Mechanical Engineering. I would have never gone down this path if Dr. Gordon did not guide me to it.

I would also like to thank the students in the Mechanics of Materials Research Group at UCF. I’d like to give a special thanks to Kevin Smith and Thomas Bouchenot. With their patience and guidance, I was able to successfully develop the codes necessary for this simulation. Without the help of these individuals, I would not have completed this work. Thank you all.

Table of Contents

List of Figures

List of Tables

1. Introduction

In various mechanical and aerospace applications, metals, ceramics, and composites are joined by various types of adhesives. These bonds are subjected to high mechanical loads during regular operation which leads to the development of shear stresses causing crack propagation and debonding. In order to compensate for these forces, adhesives with appropriate strength must be selected; however, it is crucial that the chosen adhesive possesses the optimal properties to allow durable and high joint strength. Certain adhesives create stronger bonds with specific materials and a joint made with an adhesive which does not effectively adhere to the chosen materials will lead to premature failure.

In order to evaluate mechanical properties, single-lap shear experiments performed in prior studies at UCF were modeled utilizing finite element analysis (FEA). The tests were performed according to the American Society of Testing and Materials (ASTM) standards and follow the ASTM standard D1002 for single-lap shear testing under tension loading. The parent materials chosen for these simulations are aluminum, stainless steel, and cold rolled steel.

2. Background

2.1 Lap Shear Testing of Adhesives

Lap shear testing is a very common choice when analyzing strengths of adhesives. As previously discussed, a single-lap joint consists of a thin adhesive layer placed between the adherends which are metal, rectangular tabs. Naturally, adhesively bonded joints withstand shear forces more efficiently than peel stresses [1]. To ensure that the joint does not experience excessive peel stresses, various testing parameters must be considered. The strength of the adhesive bond greatly depends on geometry, testing rate, adherend material, properties of the adhesives, overlap length, and several other components of the joint. Of all the mentioned characteristics, it has been found that the overlap length has the greatest effect on the joint strength [2]. However, much attention has been given to the thickness of the bondlines. When the bondlines are thin, the lap joint strength has been observed to increase. The reason for this being that a thick bondline contains more defects such as voids and microcracks [3] which lead to a weaker bond. Throughout the lap shear test, the joint is subjected to an in-plane tensile load and a linear shear stress distribution is seen throughout the thickness of the adherends [1]. Consequently, eccentricities in the load path cause deformation of the adherends and the internal moment at the edge of the overlap region is reduced as the experiment progresses. This reduction in moment directly influences the distribution of shear and peel stresses in the adhesive layer and the resulting problem may require a nonlinear solution [1].

Many analytical models have been made throughout the history of lap shear testing. The first method found in literature for stress analysis of bonded joints was created by Volkersen in 1938. Throughout his work, he developed the “shear-lag model” which introduced the idea of differential shear but neglected the bending effect due to the eccentric load path [4]. The first to take the deflection of the adherends into account and treat them as elastic members as opposed to rigid bodies were Goland and Reissner. They observed that in addition to the applied tensile load per unit width ($\bar{P}$), the joint ends are subjected to a bending moment (M), and a transverse force (V) due to the eccentric load path of a single-lap joint [5]. Using a bending moment factor (k) and a transverse force factor (k'), they formulated the following relations:

$$M = k\frac{\bar{P}t}{2}$$

$$V = k'\frac{\bar{P}t}{c}$$

where t is adherend thickness $(t_1 = t_2)$, and c is half of the overlap length [5]. Their experiments yielded the following expression for the bending moment factor:

$$k = \frac{\cosh(u_2 c)}{\cosh(u_2 c) + 2\sqrt{2}\sinh(u_2 c)}$$

where

$$u_2 = \sqrt{\frac{3(1-v^2)}{2}}\frac{1}{t}\sqrt{\frac{\bar{P}}{tE}}$$

where E is Young's modulus of the adherends and v is the Poisson's ratio of the adherends. To reduce the complexity of the solution, the adhesive layer was considered to have negligible thickness.

After the solution found by Goland and Reissner, Hart-Smith modified their experiments by observing the behavior of the upper and lower adherends in the overlap region individually.

This introduced the adhesive layer into the solution and produced an enhanced expression for Goland and Reissner's bending moment factor:

$$k = \left(1 + \frac{t_a}{t}\right) \frac{1}{1 + \xi\, c + \frac{1}{6} (\xi\, c)^2}$$

where t_a is the adhesive thickness, $\xi^{\,2} = \frac{\bar{P}}{D}$, and D is the adhereneds bending stiffness [5].

2.2 Finite Element Modeling of Lap Shear Tests

To simulate single-lap shear tests, numerical modeling represents a viable option. Finite element method determines approximate solutions to partial differential equations (PDEs) and applies the selected parameters to small elements known as finite elements throughout the entire geometry of the object. When lap shear tests are simulated via finite element modeling, the adhesive is assumed to provide cohesive tractions across the interface joint [5]. Previous models have used two-dimensional plane-stress elements to represent the adherends. The contact zone has been assumed to exhibit linear-elastic behavior until yielding occurs and once yielding occurs, it exhibits isotropic hardening [6].

3. Experimental Approach

Testing was performed on specimens provided by Engineering Bonding Solutions, LLC. Data collected from testing was used to compare the validity of the FE results. The provided samples were developed to comply with the ASTM D1002 test method. The adherend dimensions are shown in Figure 1, where *L* is the length of the overlap region. The bond gap for the provided samples ranges from 0.254 mm to 0.305 mm.

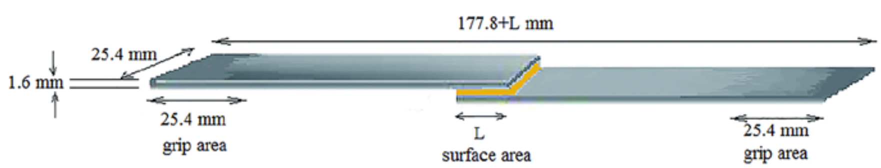

Figure 1: Specimen Dimensions

As stated by the ASTM D1002 standard test method, the grip area must be a 1 inch by 1 inch square and must be sufficiently tightened to prevent slipping during testing. The material testing machine utilized for the single-lap shear experiments was an Instron equipped with a 50kN capacity load cell (Figure 2). The free crosshead speed for the testing machine was maintained at 1.3 mm (0.05 in)/min. The adherend materials included aluminum, cold rolled steel, and stainless steel. Although these three metals were tested, the focus of the simulations and this thesis will be on the aluminum samples. Methacrylate adhesives of various chemical compositions (SA1-30-MOD, SA10-100, and SA10-05) were used to adhere the metallic tabs.

Microsoft Excel.

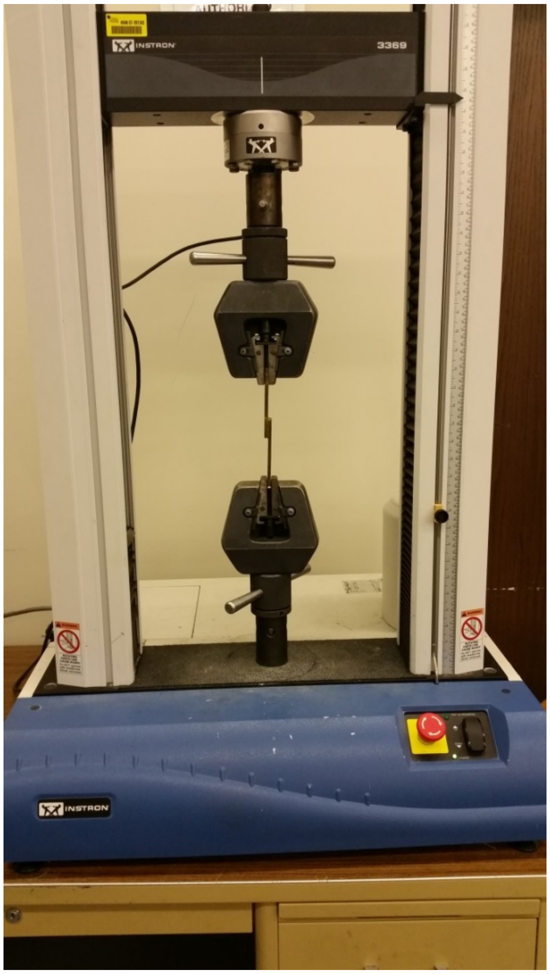

Figure 2: Instron 50kN Electromechanical Load Frame

Upon completion of the experimental setup, the Instron machine is set to apply a tensile load on the clamped sample and elongates the specimen until the adhesive experiences either adhesive or cohesive failure, shown in Figure 3 below. To ensure that the adhesive bond possesses desirable strength, it is crucial to observe not only when the adhesive layer fails but also how it is failing. With the ruptured sample and a clear representation of how the adhesive tends to fail, the data outputted by the Instron software was extracted and analyzed using Microsoft Excel.

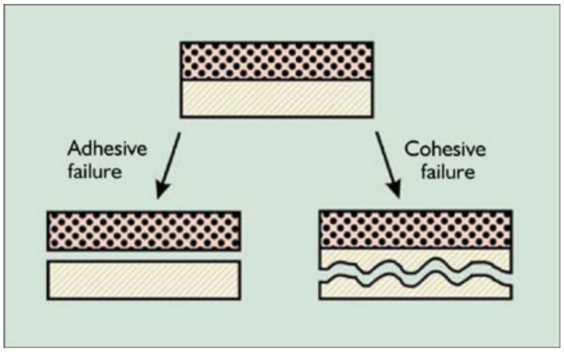

Figure 3: Cohesive and Adhesive Failure Modes

Examples of each failure mode found in the experimental results are presented below. As can be observed, for adhesive failure, the chemical bonds at the adherend-adhesive interface become weaker than the adhesive strength of the adhesive. This causes the residual adhesive to remain on one surface of the joint only. During cohesive failure, the specimen fails along the thickness of the ahesive layer. This is typically caused by insufficient overlap length or excessive peel stresses [7]. In this case, the residual adhesive remains on both surfaces.

Figure 4: Mixed Mode Failure (Adhesive and Cohesive)

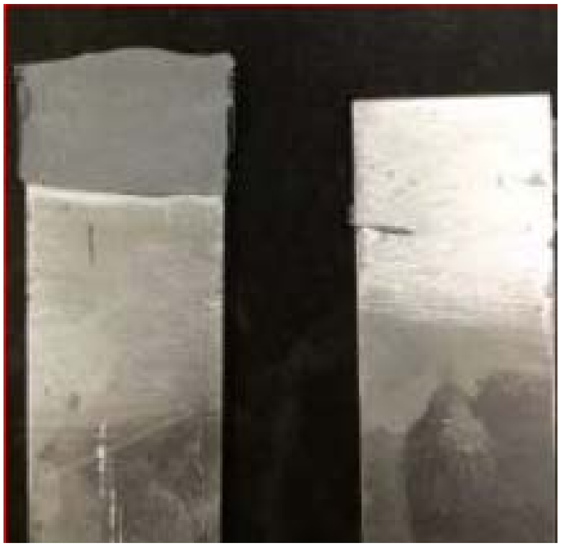

Figure 5: Adhesive Failure

Adherend failure occurs due to in-plane stresses resulting from the direct load stresses and bending stresses which are imposed due to the eccentric load path of the experiment [8]. In this failure mode, the bond between the fibers in the adherends fails prior to the adhesive, causing failure in the aherend as opposed to the adhesive layer (Figures 6, 7, and 8) .

Figure 8: Initial Loading

Figure 7: Bending Moment

Figure 6: Adherend Failure

Adhesive	Adherend	ASTM Standard	Number of Specimens
SA10-05	AL, CRS, SS	D 1002	4
SA1-30A	AL, CRS, SS	D 1002	6
SA1-305	AL, CRS, SS	D 1002	5
SA1-05	FRP	D 5868	5
SA1-05A	AL, CRS, SS	D 1002	6

Figure 9: Summary of Experiments

Presented above is a summary of the experiments run in the MOMRG lab. Due to the primary purpose of these experiments being for industry and for creating a marketable product, the composition of each adhesive was not disclosed. As can be seen on each specimen composed of metal-to-metal bonds, each adhesive which follows the ASTM D1002 standard is tested on aluminum (AL), cold rolled steel (CRS), and stainless steel (SS). Each specimen analyzed with the ASTM D5868 standard contained fiberglass reinforced plastic (FRP). The single base methacrylate specimens were provided by Engineering Bonding Solutions, LLC and are known as ACRALOCK structural adhesives. Some data for a small amount of these adhesives is available through the ACRALOCK website. Since the mechanical properties of SA10-05 are provided by the datasheet online and were known through personal inquiry of the customer, this adhesive is chosen as the focus of this research.

Figure 10: SA10-05 Specimen with AL Adherends

The adherend chosen for analysis is aluminum (Figure 10). The modulus of elasticity of aluminum 6061-T6 is known to be 68.9 GPa. The Poisson's ratio is 0.33. For the SA10-05 adhesive, the modulus of elasticity and Poisson's ratio (provided by supplier) are 620 MPa and 0.48, respectively. When combined, an adhesive layer of SA10-05 with aluminum adherends is expected to have shear strength of 17.2 – 20.7 MPa.

The raw data obtained from the Instron acquisition software is shear force and shear displacement data. Figure 11 shows plotted data raw data for the specimen made up of aluminum adherends and the SA10-05 adhesive.

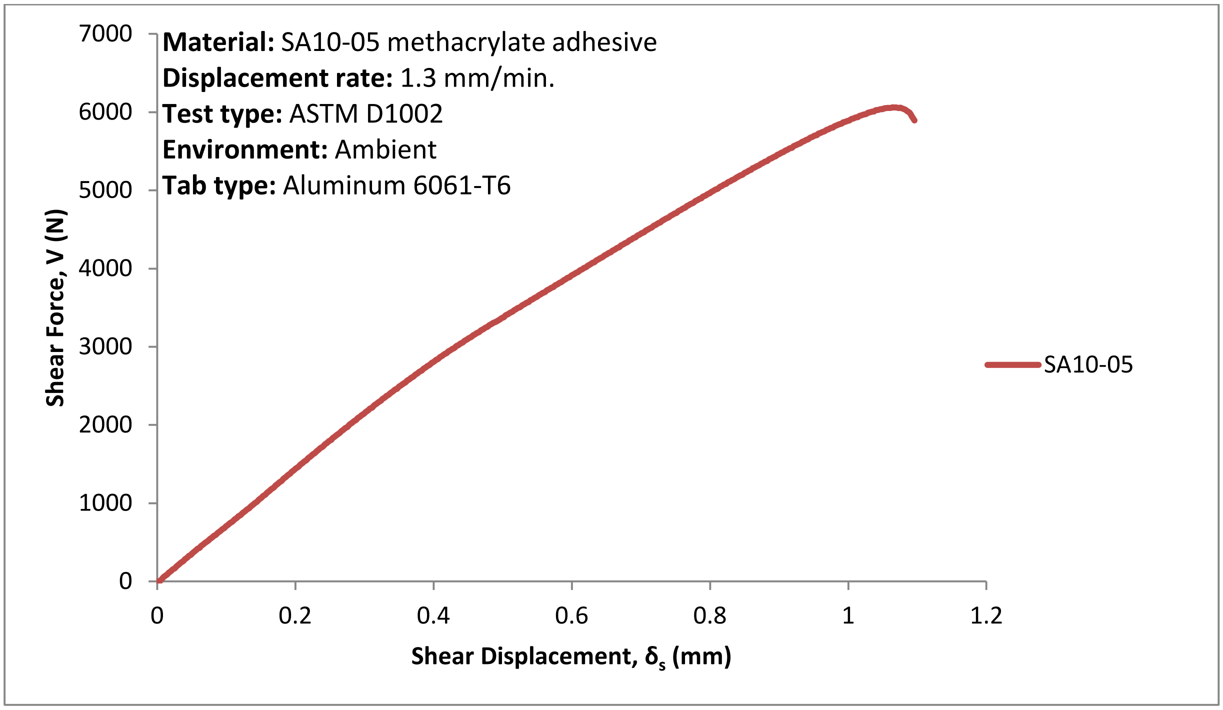

Figure 11: Shear Force vs. Shear Displacement

To further analyze the results, shear stress and shear strain were calculated using the following equations:

$$\tau = \frac{V}{bL}$$

$$\gamma = \frac{d_a - d_m}{t}$$

where τ is engineering shear stress, V is shear force, b is the joint width, L is the joint length, γ is engineering shear strain, d_a is the displacement measured on the test sample, d_m is the corrected displacement of the adhered, and t is the thickness of the adhesive layer [9]. Due to the nature of this experiment, d_m contributes a negligible amount of displacement and is therefore neglected. The data curve for shear stress versus shear strain is shown below in Figure 12.

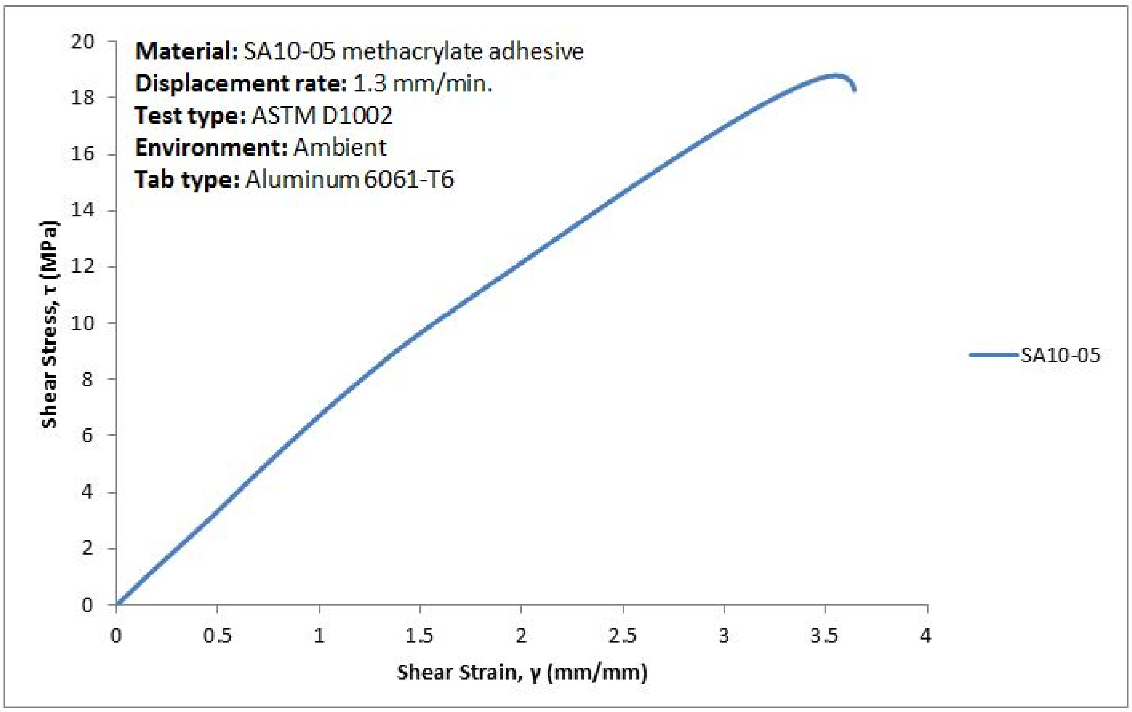

Figure 12: Shear Stress vs. Shear Strain

For the specific specimen in question, four trials were run. The data was collected for each run and data analysis was conducted on the results. The collection of results is shown below, in Figure 13.

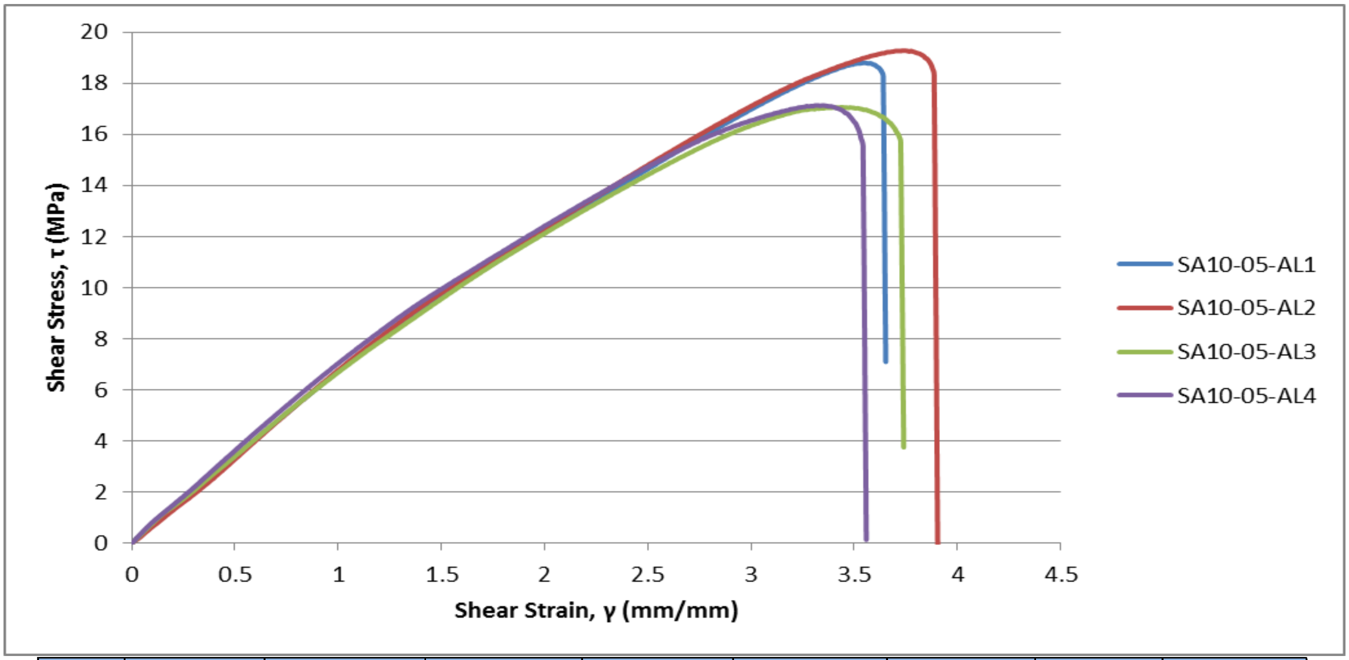

Sample	Width(mm)	Length(mm)	Area (mm^2)	Load at Failure (N)	Yeild Strength (MPa)	Extension at Failure (mm)	Strength at Break (MPa)	Failure (C/A)
1	25.4	12.7	322.58	6064.281359	18.79930981	1.09601	18.278427	COHESIVE
2	25.4	12.7	322.58	6218.509013	19.2774165	1.171575	18.334233	COHESIVE
3	25.4	12.7	322.58	5503.860776	17.06200253	1.1219942	15.698948	COHESIVE
4	25.4	12.7	322.58	5526.684519	17.13275627	1.0676128	15.545989	COHESIVE
Mean	**25.4**	**12.7**	**322.58**	**5828.333917**	**18.06787128**	**1.114298**	**16.964399**	
St. Dev	0	0	0	367.0526664	1.137865542	0.044173314	1.5509535	
COV	0	0	0	6.297728848	6.297728848	3.96422808	9.1424015	

Figure 13: Collection of Experimental Data

4. Numerical Approach

4.1 Specimen Design

The finite element model developed in ANSYS uses three dimensional structural solid elements, specifically SOLID185 eight-noded elements (Figure 14). Both the adherends and adhesives were modeled utilizing this element type. To simulate the adhesion between the faces of the adherends and the adhesive, eight-noded linear interface elements (INTER205) were used (Figure 15). Using eight-noded elements as opposed to twenty-noded elements significantly reduced both the complexity and solution time of the simulation.

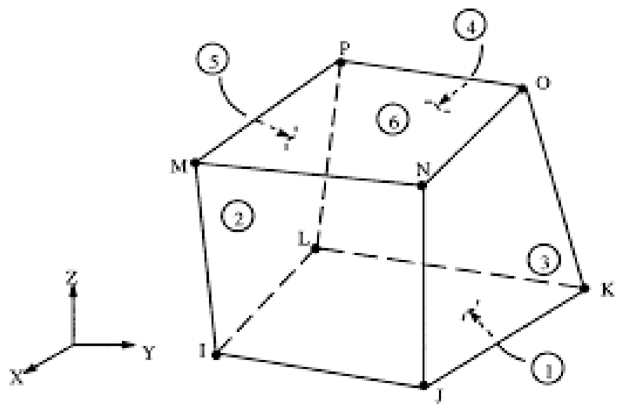

Figure 14: SOLID185 3-D 8-Node structural solid elements

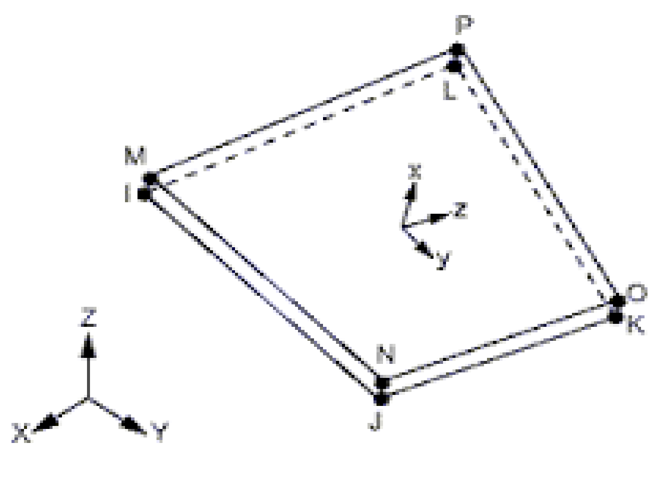

Figure 15: INTER205 3-D 8-Node linear interface elements

Due to the geometry of the model, it is convenient to use symmetry in order to further reduce the complexity of the model. The number of elements was halved by mirroring the model along the centerline of the y-axis, denoted in Figure 16 by a capital S. In a previous study conducted by Kashif [10], it was found that the stresses and their gradients are high at or near the ends of the overlap region. The critical regions are located at the adherend-adhesive interfaces making it necessary to create a mesh with small elements across this area. This allows for accurate solutions and employing this mesh refinement method through the thickness of the specimen allows for the analysis of the stresses experienced through the thickness of the adhesive. The level of refinement is shown in Figure 17.

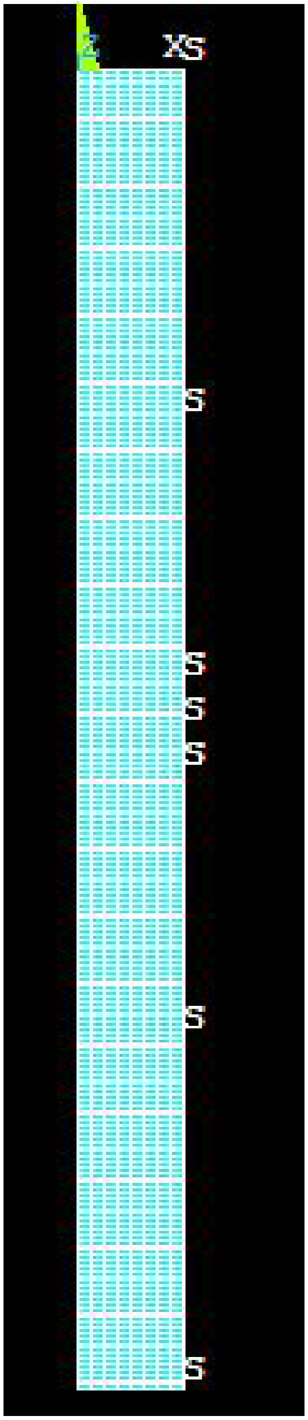

Figure 16: Representation of Model Symmetry

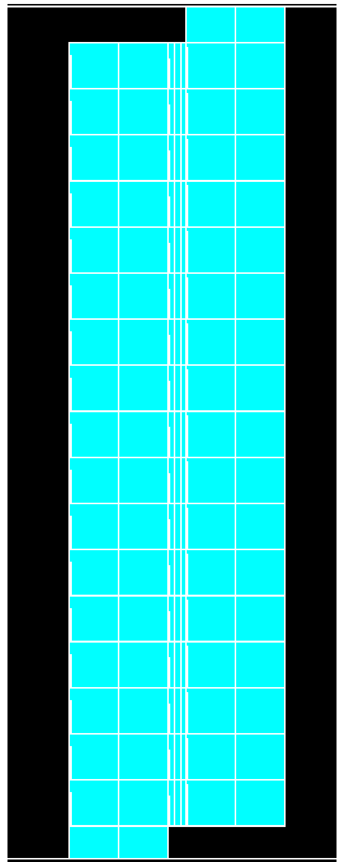

Figure 17: Representation of Mesh Refinement

As previously mentioned, this finite element model utilizes the cohesive zone model (CZM) to simulate the adhesive layer. In order to correctly create the interface elements required by the cohesive zone approach, the elements along the xy-plane at the adherend-adhesive interface must align perfectly. For this reason, a hexahedral mesh is used. The exponential law for traction separation is followed, incorporating three material constants (Table 1). This particular cohesive zone law is attractive to researchers because a phenomenological description of contact is automatically achieved in normal compression and the tractions and their corresponding derivatives are continuous [11].

Constant	Meaning	Property
C1	σ_{max}	Maximum normal traction at the interface
C2	δ_n	Normal separation across the interface where the maximum normal traction is attained
C3	δ_t	Shear separation where the maximum shear traction is attained

Table 1: Exponential Cohesive Zone Law Material Constants [ANSYS Help Menu]

In the Experimental Results chapter, the presence of plastic deformation and the yield point observed in the experimental data curves was discussed. To account for this, the bilinear kinematic hardening (BKIN) material model was utilized. As previously stated, the BKIN material model incorporates the yield stress and the tangent modulus into the simulation (Table 2). Due to its ability to incorporate the Bauschinger effect and account for the material softening in compression, BKIN was chosen over bilinear isotropic hardening (BISO) which assumes that yield stress in compression increase at the same rate as yield stress in tension [12].

Constant	Meaning	Property
C1	σ_0	Initial yield stress
C2	E_T	Tangent modulus

Table 2: Bilinear Kinematic Hardening Material Model Constants [ANSYS Help Menu]

From the experimental setup pictured previously, it can be observed that the specimen is constrained in both the x and the z directions at the top and bottom of the sample. The regions lying between the clamped areas are left to deflect freely. The testing machine displaces the single-lap shear joint in the y direction. In order to simulate the constraints imposed on the specimens during the experiments, the boundary conditions shown in Figure 18 are included in the simulation. The lower bound of the modeled specimen is fixed while the upper bound is allowed to translate freely in the y direction, accounting for the displacement induced by the testing machine.

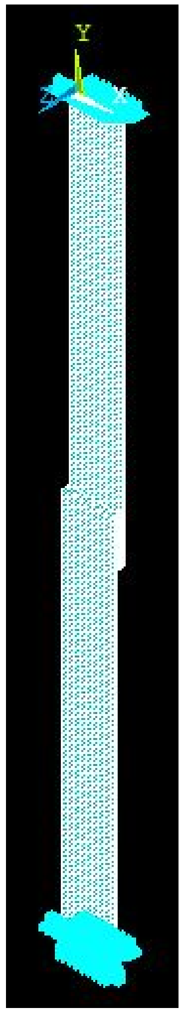

Figure 18: Boundary Conditions

4.2 Determining Material Constants

Each material model included in this simulation requires various material constants to be inserted into the APDL code. In order to optimize the simulation and obtain accurate data, initial guesses were chosen arbitrarily for each parameter. The simulation was run with these chosen values and the data was stored. An iterative method, similar to the procedure used in a study requiring traction-separation material parameters [13], in which each parameter was varied by equal increments was then implemented to optimize the values. The results obtained from the simulations were compared to the experimental data and modified until the simulation and the experimental curves were considerably similar.

With the simulation curve possessing similar qualities as the experimental data curve, the simulation parameter values were then varied further and inserted into a Taguchi array. An L25 orthogonal array was utilized to automate the iterative process, reducing the number of experiments significantly. Table 3 shows how each experiment was determined, with *P* representing a model parameter. Table 4 indicates the initial values used for the simulations and Table 5 shows the varied values for each parameter.

Experiment	$P1$	$P2$	$P3$	$P4$	$P5$	$P6$
1	1	1	1	1	1	1
2	1	2	2	2	2	2
3	1	3	3	3	3	3
4	1	4	4	4	4	4
5	1	5	5	5	5	5
6	2	1	2	3	4	5
7	2	2	3	4	5	1
8	2	3	4	5	1	2
9	2	4	5	1	2	3
10	2	5	1	2	3	4
11	3	1	3	5	2	4
12	3	2	4	1	3	5
13	3	3	5	2	4	1
14	3	4	1	3	5	2
15	3	5	2	4	1	3
16	4	1	4	2	5	3
17	4	2	5	3	1	4
18	4	3	1	4	2	5
19	4	4	2	5	3	1
20	4	5	3	1	4	2
21	5	1	5	4	3	2
22	5	2	1	5	4	3
23	5	3	2	1	5	4
24	5	4	3	2	1	5
25	5	5	4	3	2	1

Table 3: Taguchi L25 Orthogonal Array

Parameters	Initial Values
$\sigma_{max}\ (Mpa)$	18.8
$\delta_n\ (mm)$	0.14
$\delta_t\ (mm)$	0.3
$\sigma_0\ (MPa)$	16
$E_T\ (MPa)$	80
$E\ (MPa)$	620

Table 4: Initial Values for Taguchi Array

Parameters	1	2	3	4	5
$\sigma_{max}\ (Mpa)$	18.8	14.1	16.45	21.15	23.5
$\delta_n\ (mm)$	0.14	0.105	0.1225	0.1575	0.175
$\delta_t\ (mm)$	0.3	0.225	0.2625	0.3375	0.375
$\sigma_0\ (MPa)$	16	4	8	24	28
$E_T\ (MPa)$	80	60	70	90	100
$E\ (MPa)$	620	465	542.5	697.5	775

Table 5: Varied Values for Taguchi Array

5. Numerical Results

Prior to running the simulations, the values indicated by Table 5 were inserted into the arrangement provided by the Taguchi L25 orthogonal array. Table 6 is the completed table with all of the levels containing the parameter values tested.

Run	$\sigma_{max}\ (Mpa)$	$\delta_n\ (mm)$	$\delta_t\ (mm)$	$\sigma_0\ (MPa)$	$E_T\ (MPa)$	$E\ (MPa)$
1	18.8	0.14	0.3	16	80	620
2	18.8	0.105	0.225	4	60	465
3	18.8	0.1225	0.2625	8	70	542.5
4	18.8	0.1575	0.3375	24	90	697.5
5	18.8	0.175	0.375	28	100	775
6	14.1	0.14	0.225	8	90	775
7	14.1	0.105	0.2625	24	100	620
8	14.1	0.1225	0.3375	28	80	465
9	14.1	0.1575	0.375	16	60	542.5
10	14.1	0.175	0.3	4	70	697.5
11	16.45	0.14	0.2625	28	60	697.5
12	16.45	0.105	0.3375	16	70	775
13	16.45	0.1225	0.375	4	90	620
14	16.45	0.1575	0.3	8	100	465
15	16.45	0.175	0.225	24	80	542.5
16	21.15	0.14	0.3375	4	100	542.5
17	21.15	0.105	0.375	8	80	697.5
18	21.15	0.1225	0.3	24	60	775
19	21.15	0.1575	0.225	28	70	620
20	21.15	0.175	0.2625	16	90	465
21	23.5	0.14	0.375	24	70	465
22	23.5	0.105	0.3	28	90	542.5
23	23.5	0.1225	0.225	16	100	697.5
24	23.5	0.1575	0.2625	4	80	775
25	23.5	0.175	0.3375	8	60	620

Table 6: Completed L25 Taguchi Array

Each level of the Taguchi array was run for 100 time steps allowing enough points to be collected to capture the behavior of the adhesive immediately before rupture. Examples of the simulation data obtained from the Taguchi experiments are shown in Figures 19, 20, and 21 below.

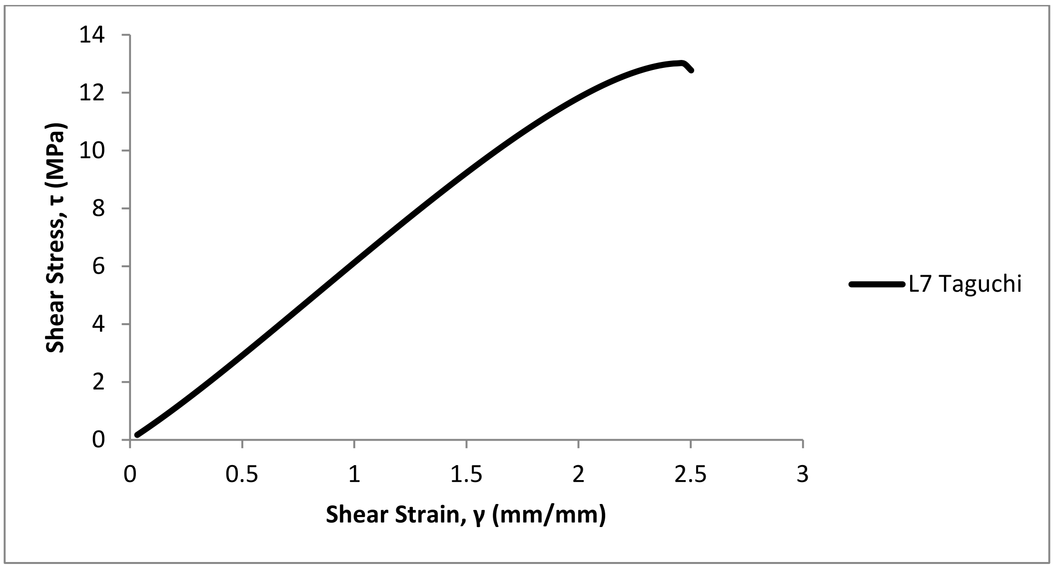

Figure 19: Numerical Solution for Level 7

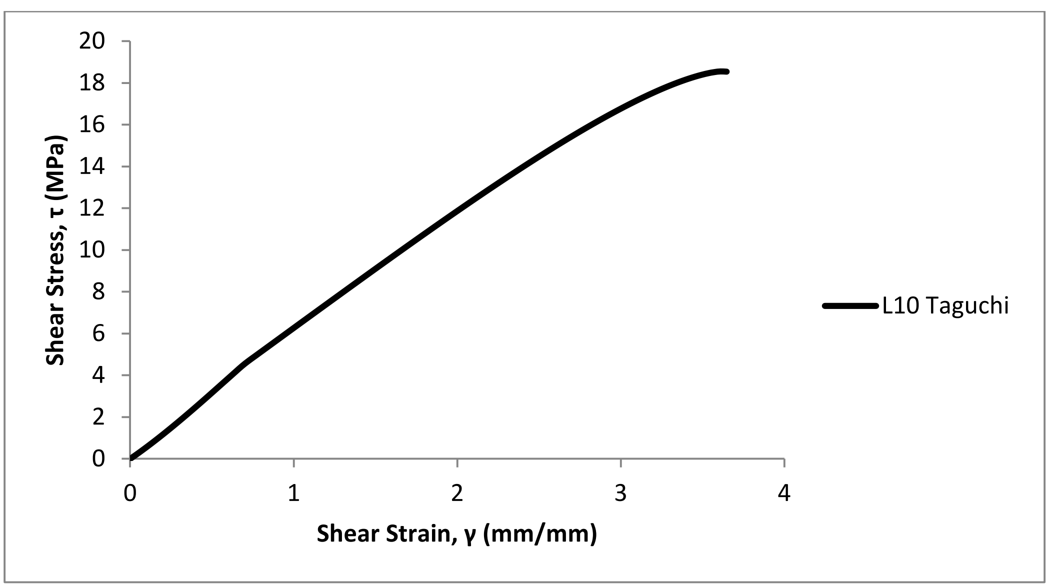

Figure 20: Numerical Solution for Level 10

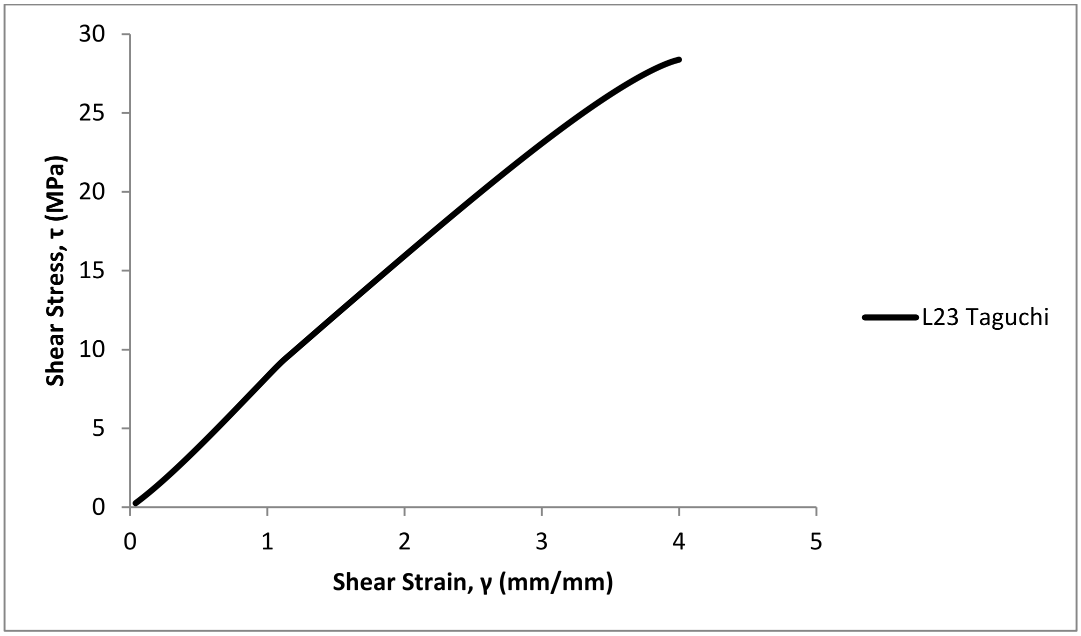

Figure 21: Numerical Solution for Level 23

By noting the difference in values shown in the completed Taguchi array and observing the data curves presented above, it is clear that even slight changes in the values of the parameters alter the entire shape.

Along with the force and displacement output of the simulation, many other aspects of the numerical solution were studied. In order to validate the simulation, results were compared to findings in similar studies. The first portion of the verification process was the deflected shape of the specimens immediately before rupture. Since it has been found that an eccentric load imposed on a single-lap joint generates bending moment and transverse force [14] evidence of adherend bending and adhesive debonding is expected. This phenomenon of rotating adherends, first considered by Goland and Reissner in 1944, is illustrated in Figure 22. Figure 23 shows the deflected shape of a single-lap joint with a 0.254 mm adhesive layer thickness observed in a previous study.

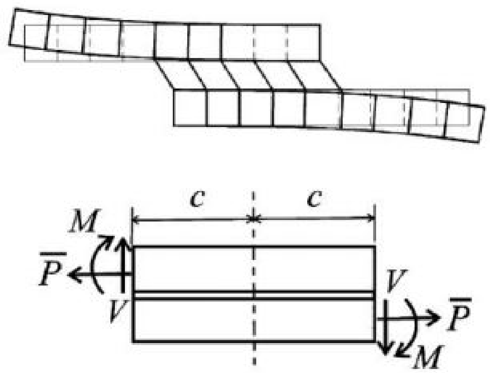

Figure 22: Rotating Adherends (Goland and Reissner, 1944)

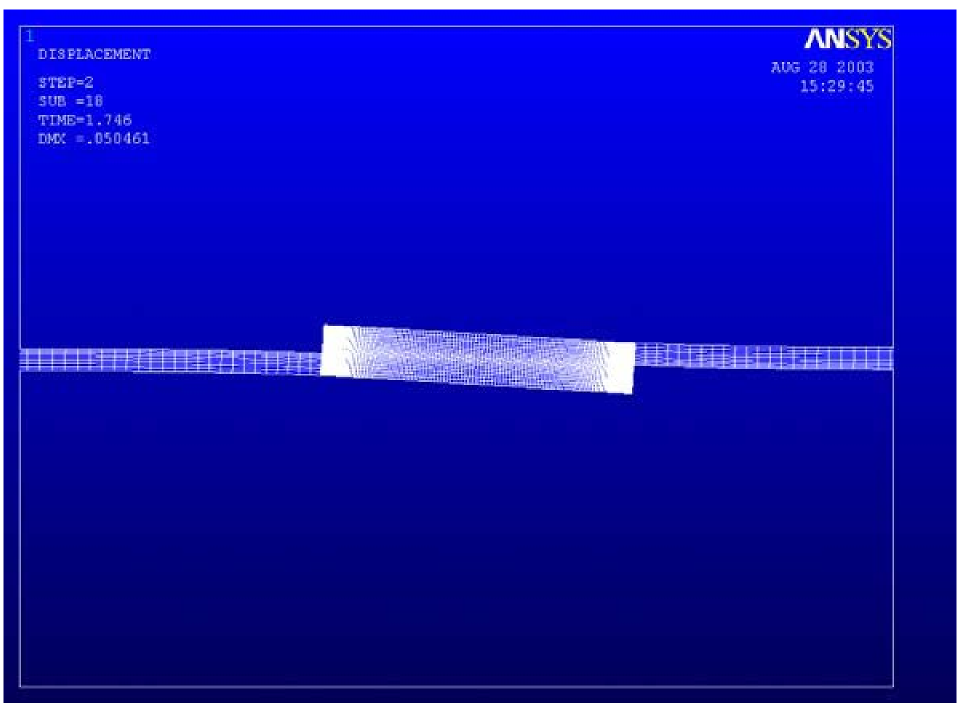

Figure 23: Deformed Shape of Single-Lap Joint [8]

A comparison between what is found in literature and the results obtained from the FE model presented here shows an agreement in the solutions. Figures 24 and 25 show the undefelcted shape of the simulated specimen and the deformed shape immediately before rupture, respectively.

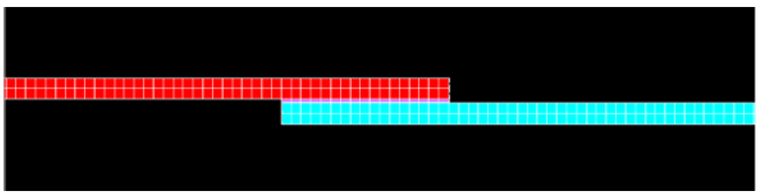

Figure 24: Undeflected FE Model

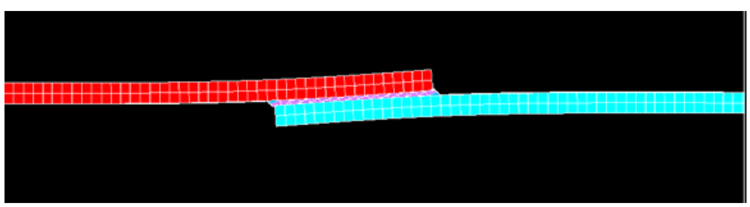

Figure 25: Deflected FE Model

Knowing that the deflected shape resembles what is seen in literature, the comparison can be expanded to include an analysis of the observations seen on the adherend- adhesive interface and within the adhesive layer. Considering the nature of the single-lap shear experiment and the geometry of the specimen, it is crucial that peel stresses be kept at a minimum to avoid premature failure. To further validate the simulation, a study of the peel stresses experienced by the upper interface of the adhesive and the adherend was conducted. When compared to what has been found in prior studies, it is seen that the simulation produces peel stress data similar to what is expected from a single-lap specimen. Figures 26 and 27 show the peel stress distribution found in literature and the simulation data, respectively.

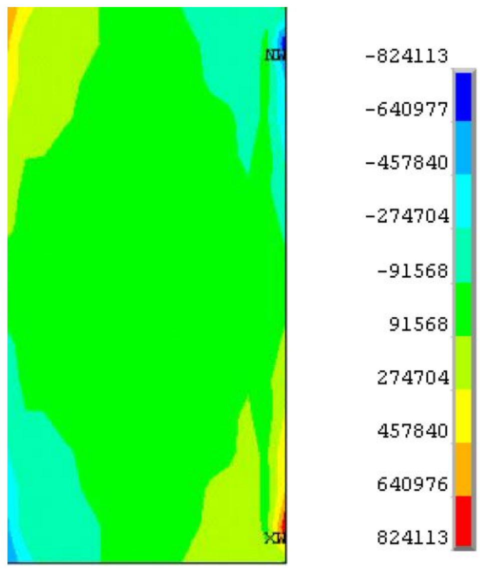

Figure 26: Peel Stress Distribution [10]

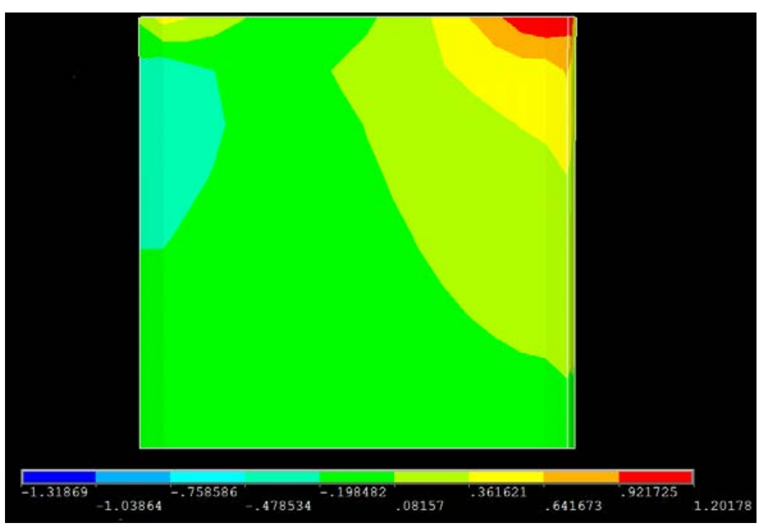

Figure 27: Simulation Peel Stress Distribution

6. Comparing Numerical and Experimental Solutions

With the assurance that the simulation was providing reasonable results, considerable effort was put into obtaining simulation data which closely matched the experimental data. Since a collection of data from simulations run for each level of the Taguchi array was present, the simulation data was plotted on the same axis as the experimental data for each run (Figures 28, 29, and 30).

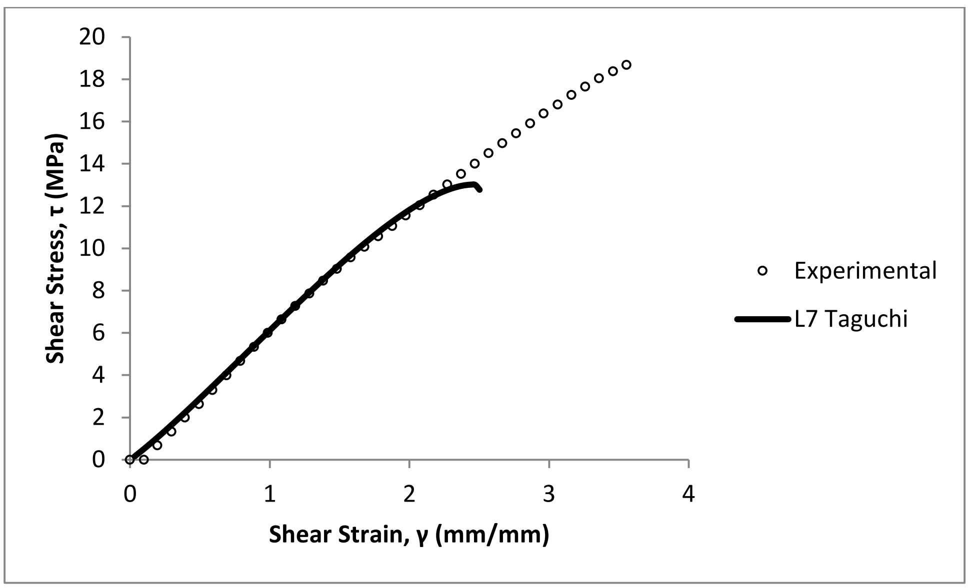

Figure 28: Comparison Between Experimental and L7 Simulation Data

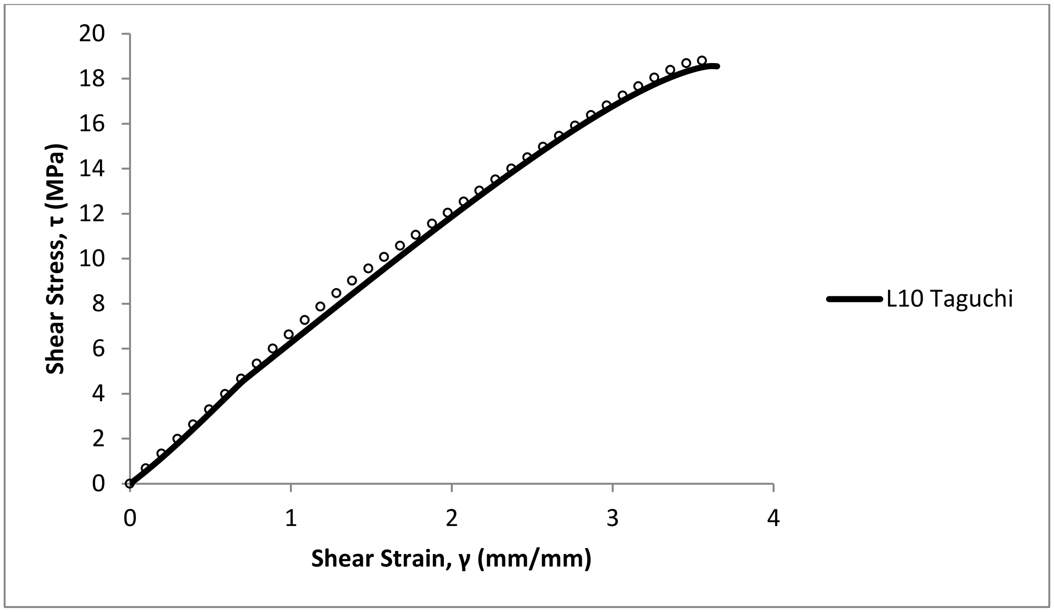

Figure 29: Comparison Between Experimental and L10 Simulation Data

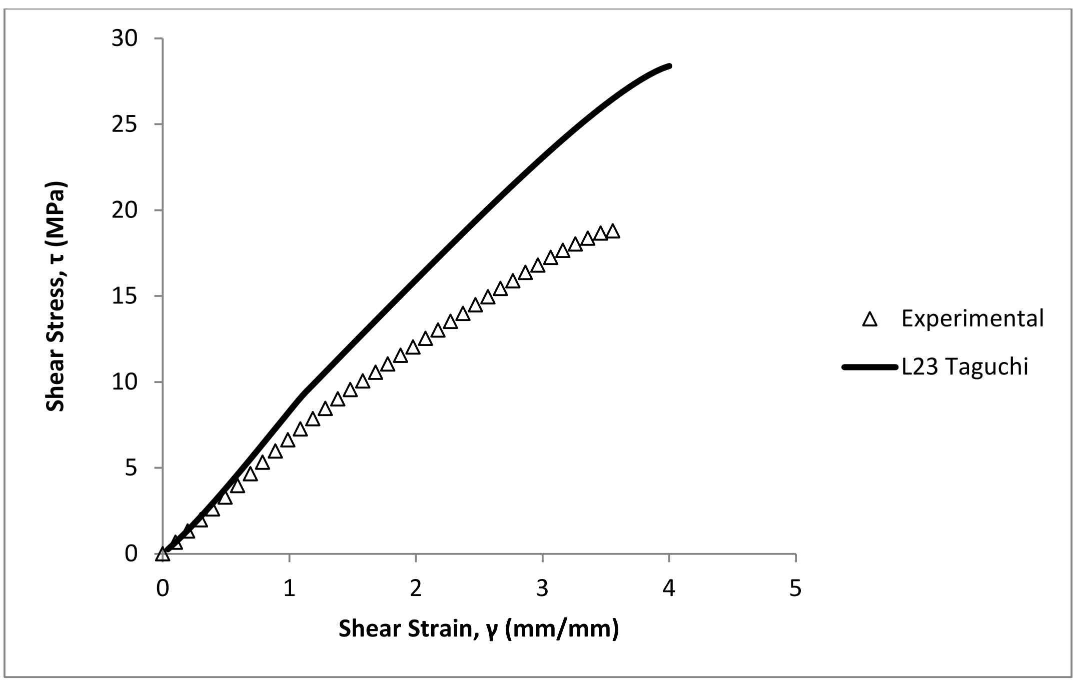

Figure 30: Comparison Between Experimental and L23 Simulation Data

Considering every level of the Taguchi array and the results obtained from each, it is obvious that level 10 provides the most accurate solution (Figure 29). The initial slope (elastic modulus) for the elastic region matches the experimental data curve closely. Upon reaching the yield stress and entering the region where plastic deformation occurs, a similar tangent modulus is found between both curves. As the specimen approaches the point of rupture, the experimental data and the simulation data both reach their ultimate strengths at approximately 18.8 MPa.

Throughout the numerical simulation procedure, a trend was seen where iterations were performed until the parameters were optimized. This method, although effective, is tedious and requires an extensive amount of time. In order to reduce experiment time and make the process more convenient, mathematical models were developed with respect to τ and the other with respect to γ.

$$\tau = \frac{\gamma}{\delta_s} + \gamma\sigma_{max}\delta_n + \frac{\gamma\sigma_{max}\delta_n\delta_0 - \sigma_{max}\delta_s\gamma^3}{E_T}$$

$$\gamma = \frac{\tau\delta_s}{(\delta_s E_T + \sigma_{max}\delta_s\delta_0 - \tau)^{\delta_n}}$$

Below, the curves obtained from the mathematical models, the simulation curves, and the experimental data are plotted on the same axis for three selected Taguchi levels (Figures 31, 32, and 33). Although the ultimate goal of the mathematical modeling effort is to obtain an equation which fits the elastic and plastic regions, along with the rupture, it can be seen that the mathematical models do follow the data quite well. Through the use of these equations, estimates of the cohesive zone and bilinear kinematic hardening models can be obtained. These values can be used to significantly reduce the time necessary to obtain an accurate numerical solution.

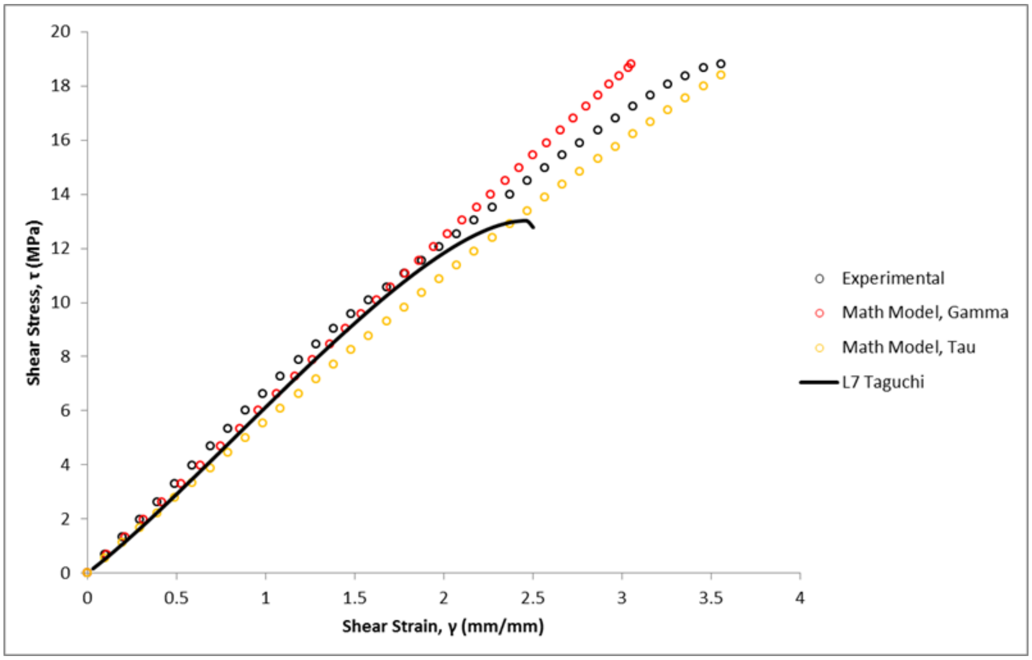

Figure 31: Experimental, Numerical, and Mathematical Modeling Curves for L7

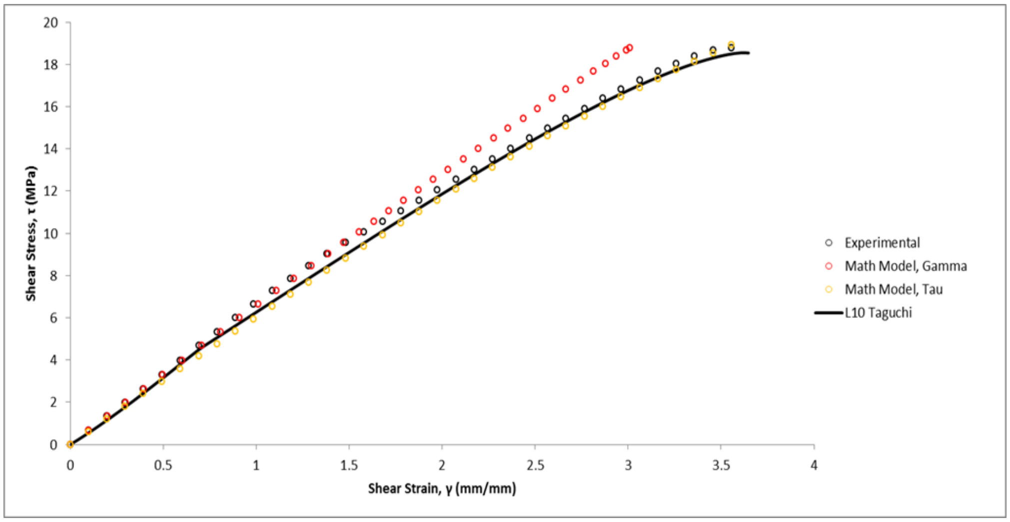

Figure 32: Experimental, Numerical, and Mathematical Modeling Curves for L10

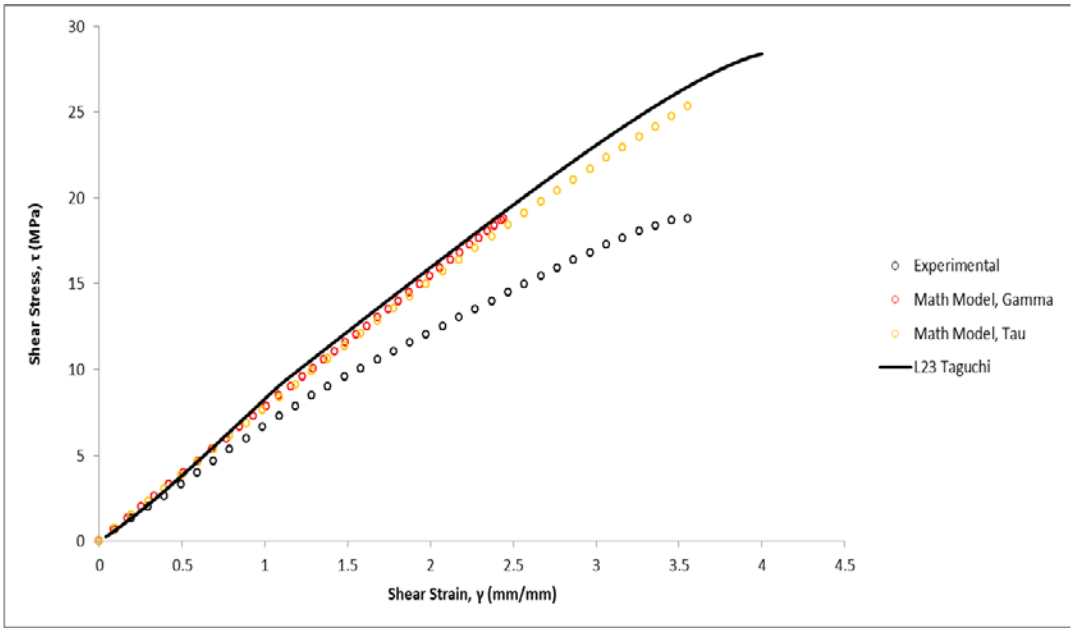

Figure 33: Experimental, Numerical, and Mathematical Modeling Curves for L23

7. Conclusions

The goal of this research is to provide a method to numerically understand the mechanical properties of adhesives. Through the use of FEA simulations, numerical results for single-lap shear tests were obtained and compared to experimental data. By doing so and comparing to results found in literature, the model was validated and it was assured that accurate results were being acquired. The FEA model made use of the cohesive zone method (CZM) to model the adhesive layer. In order to account for the yield stress and the plastic deformation, the bilinear kinematic hardening (BKIN) material model was employed. By implementing these modeling techniques, creating a mathematical model utilizing the simulation data and comparing each result, a valid approach to observe the behavior of single-lap joints is created and the mechanical properties of adhesive layers are thoroughly explored to better understand adhesive bonding and optimize bond strength.

Appendix

```
finish
/clear
/PNUM,TYPE,1
/title, Tensile Test Redo
/prep7

ET,1,SOLID185
ET,2,SOLID185
ET,3,SOLID185

MP,EX,1,6.9E4            ! Young's modulus (Material 1 - N/mm^2)
MP,PRXY,1,0.334          ! Poisson's ratio (Material 1)

MP,EX,2,620
!MP,GXY,2,21.692              ! Young's modulus (Material 2 - N/mm^2)

MP,PRXY,2,0.48
TB,BKIN,2
TBDATA,,4,60             !BKIN

MP,EX,3,6.9E4            ! Young's modulus (Material 3 - N/mm^2)

!MP,GXY,3,2.4E4           ! Shear Modulus (N/mm^2)

MP,PRXY,3,0.334

TYPE,1

BLOCK,0,12.7,0,-101.6,0,1.6

Mat, 1

mshape,0,3D                   ! Differentiate between Textra- and Hexa-

TYPE,1
LESIZE,7,,,8
LESIZE,11,,,2
LESIZE,6,,,136
VMESH,1
DA,      6,SYMM
TYPE,2

BLOCK,0,12.7,-88.9,-101.6,1.6,1.9
```

```
Mat,2

TYPE,2
LESIZE,18,,,17
LESIZE,22,,,3
LESIZE,19,,,8
VMESH,2

DA,     12,SYMM

TYPE,3

BLOCK,0,12.7,-88.9,-190.5,1.9,3.5

Mat,3

TYPE,3
LESIZE,29,,,8
LESIZE,34,,,2
LESIZE,30,,,136
VMESH,3

DA,     18,SYMM

ESEL,S,TYPE, ,2
NSLE
NSEL,R,LOC,Y,-88.9,-101.6
CM,ADH1,NODE,
NSEL,S,LOC,Y,0
CM,TOP_1,ELEM,


NSEL,S,LOC,Y,0
CM,TOP1,NODE,

ESEL,S,TYPE,,1
NSEL,R,LOC,Y,0
NSEL,R,LOC,X,0
CM,TOPSING,NODE

ESEL, S, TYPE, ,3                 !Select a subset of elements
NSLE                              !Select nodes associated with above elements
NSEL,R,LOC,Y,-101.6
```

```
CM,  TOP3, NODE,

NSEL, S, LOC, Y, -190.5
CM,  BASE3, NODE,
ALLSEL,ALL
TNMAX=23.5
delta_norm=0.175
delt_shear=0.3375
ET,4,INTER205
TB,CZM,4,,,EXPO

TBDATA,1,TNMAX,delta_norm,delt_shear
CSYS,0

esel,s,type,,2
NSEL,R,LOC,Y,-88.9,-101.6
NSEL,R,LOC,X,12.7
!NSEL,R,LOC,Z,1.6,2.1
CM,SIDE,NODE,

ALLSEL,ALL

!*************************************************



ESEL, S, TYPE, ,1,
CM, ePlate1, Elem
ESEL, S, TYPE, ,2,
CM, ePlate2, Elem
ESEL, S, TYPE, ,3,
CM, ePlate3, Elem

ESEL, S, TYPE, ,1,2,1
NSLE
NSEL, S, LOC, Y, -88.9,-101.6, 1
NSEL, R, LOC, Z, 1.6,
NUMMRG,Nodes
Type,4
MAT,4
CZMESH, ePlate1, ePlate2,

-----------------------------------------
```

```
ESEL, S, TYPE, ,2,3,1
NSLE
NSEL, S, LOC, Y, -88.9,-101.6, 1
NSEL, R, LOC, Z, 1.9,
NUMMRG,Nodes
Type,4
MAT,4
CZMESH, ePlate2, ePlate3,

!NSEL,S,LOC,Y,-101.6
!NSEL,R,LOC,Z,2.1,3.7
!NUMMRG,NODES
!ESLN

!NSEL,S,LOC,Y,-88.9
!NSEL,R,LOC,Z,0,1.6
!NUMMRG,NODES
!ESLN



!*******************Boundary Conditions**********************

!cmsel,s,ADH1,NODE
!D,ALL,UZ,0
!D,ALL,UY,0
!D,ALL,UX,0

!cmsel,s,ADH2,NODE
!D,ALL,UZ,0
!D,ALL,UY,0
!D,ALL,UX,0

cmsel, s, top1, node
D,ALL,UZ,0
D,ALL,UX,0

cmsel, s, base3, node
D,ALL,UZ,0
D,ALL,UY,0
D,ALL,UX,0
```

```
allsel,all

/SOLU
ANTYPE,STATIC
NLGEOM,ON

cmsel, s, top1, node
!CP,NEXT,UY,ALL
!F,ALL,FY,100
D,top1,UY,1.3



ALLSEL, ALL
!TIME,20

sub_steps = 10
AUTOTS,OFF
NSUBST, sub_steps
Outres, All, All
solve
FINISH
!/EXPAND,2,RECT,HALF,12.7
!/REPLOT

!******POSTPROCESSEING*****************
!*DIM,TTime,ARRAY,TIME_count,1

/post1
/OUTPUT,WithoutBKIN,txt,C:\Users\Wilson\Desktop\Research\Results\New_Test
!*DIM,ReactionForces,ARRAY,sub_sets
RESET
cmsel,s,top1,node
NPLOT
*DO,i,0,sub_steps,1
        SET,,, ,,, ,i
        FSUM,,top1
        !PRRSOL,FY
*ENDDO

/post1
/OUTPUT,Stress_stuff,txt,C:\Users\Wilson\Desktop\Research\Results
RESET
NSEL,S,LOC,Y,-88.9,-101.6
```

```
NSEL,R,LOC,Z,2.1
NSEL,R,LOC,X,0
NPLOT

*DO,i,0,sub_steps,1
	SET,,, ,,, ,i
	!PLNSOL, S,EQV, 0,1.0
	PRNSOL,EPTO,PRIN
*ENDDO

/post1
/OUTPUT,Stress_stuff,txt,C:\Users\Wilson\Desktop\Research\Results
NSEL,S,LOC,Y,-88.9,-101.6
NSEL,R,LOC,Z,1.8
NSEL,R,LOC,X,0
NPLOT

SET,,, ,,, ,19
!*
PRNSOL,S,PRIN

/post1
/OUTPUT,Stress_stuff,txt,C:\Users\Wilson\Desktop\Research\Results
NSEL,S,LOC,Y,-88.9,-101.6
NSEL,R,LOC,Z,1.8
NSEL,R,LOC,X,0
NPLOT

SET,,, ,,, ,19
!*
PRESOL,S,PRIN
!*****************************************************************************
```

References

[1] Albuquerque, E., Paiva, W., Rodrigues, M., and Rodriguez, R., 2010, "Analytical and Numerical Tools for Bonded Joint Analysis," *Mecánica Computacional*, 29**,** pp. 7557-7569.

[2] Alía, C., Arenas, J., and Narbón, J., "Optimum Adhesive Thickness in Structural Adhesives Joints Using Statistical Techniques Based on Weibull Distribution," pp. 1-6.

[3] Brown, K., Carbas, R., Critchlow, G., Figueiredo, M., and da Silva, L., 2009, "Effect of Material, Geometry, Surface Treatment and Environment on the Shear Strength of Single Lap Joints," *International Journal of Adhesion & Adhesives*, 29 (6), pp. 621-632.

[4] Christensen, T., 1976, "A Finite Element Analysis of a Single Lap Shear Adhesive Joint With and Without an Edge Crack," pp. 48-65.

[5]Court, R., Sutcliffe, M., and Tavakoli, S., 2001, "Ageing of Adhesively Bonded Joints – Fracture and Failure Analysis Using Video Imaging Techniques," *International Journal of Adhesion and Adhesives*, 21 (6), pp. 2-3

[6] Kafkalidis, M., and Thouless, M., 2002, "The Effects of Geometry and Material Properties on the Fracture of Single Lap-Shear Joints," pp. 8-18.

[7] Davis, M.J., and Bond, D.A., "The Importance of Failure Mode Identification in Adhesive Bonded Aircraft Structures and Repairs," *Aircraft Structural Integrity Section.*

[8] Zhu, Y., and Kedward, K., 2005, "Methods of Analysis and Failure Predictions for Adhesively Bonded Joints of Uniform and Variable Bondline Thickness," Technical Report No. DOT/FAA.AR-05/12, *Federal Aviation Administration*, Washington, DC.

[9] ASTM D5656-10, Standard Test Method for Thick-Adherend Metal Lap-Shear Joints for Determination of the Stress-Strain Behavior of Adhesives in Shear by Tension Loading, ASTM International, West Conshohocken, PA, 2010,www.astm.org

[10] Kashif, S.M., (0017), "Delamination effect modeling, simulation and experimental validation of lap shear test," *International Journal of Mechanical and Materials Engineering.*

[11] Bosch, M.J., Schreurs, P.J.G., Geers, M.G.D., 2006, "An improved description of the exponential Xu and Needleman cohesive zone law for mixed-mode decohesion," *Engineering Fracture Mechanics*, 73, pp. 1220-1234

[12] Taneja, A., 2012, "On isotropic and kinematic hardening," http://www.ajaytaneja-isotropickinematichard.blogspot.com/

[13] Di Leo, C.V., Luk-Cyr, J., Liu, H., Loeffel, K., Al-Athel, K., Anand, L., 2014, "A new methodology for characterizing traction-separation relations for interfacial delamination of thermal barrier coatings," *Acta Materialia*, 71, pp. 306-318

[14] Moreira, D.C., Nunes, L.C.S., 2014, "Experimental analysis of bonded single lap joint with flexible adhesive," *Applied Adhesion Science*, 2, pp. 1-8